3D MHD Simulations of Obliquely Rotating Massive Stars

A. ud-Doula[1]

1. Penn State Scranton, 120 Ridge View Drive, Dunmore, PA 18512, USA

We present preliminary results from the most recent 3D MHD simulations of massive star winds. This is a natural extension of previously studied numerous 2D and limited field-aligned 3D MHD models. Here, we focus on how obliquity of the magnetic field with respect to the rotational axis may affect the overall dynamics of the winds. More in-depth study how obliquity affects stellar spindown time and possible variability in Halpha emission is deferred to future studies.

1 Introduction

Hot, luminous, massive stars are prominent sources of soft ($0.5 - 1\,\mathrm{keV}$) X-rays, thought to be produced by Embedded Wind Shocks (EWS) that develop from intrinsic instabilities in their line-driven winds (Owocki et al., 1988; Feldmeier et al., 1997). But in the subset of massive stars with strong magnetic fields, the stronger (several keV) X-ray emission seems better explained by magnetically confined wind shocks (MCWS), which arise from the direct collision of wind flow from opposite footpoints of closed magnetic loops (Babel & Montmerle (1997) ; see fig. 1). With the recent increase in the number of OB stars with measured surface magnetic fields (Wade et al., 2016), and with the discovery in *Chandra* surveys (Nazé et al., 2011; Townsley et al., 2011) of populations of OB stars showing hard X-ray spectra and high $L_{\rm X}/L_{\rm Bol}$ ratios, the time is ripe for a theoretical effort focused on understanding the X-ray emission properties of these magnetic massive stars. In addition, especially B stars, show evidence of Hα emission. As such, understanding these stars has become increasingly more important.

In an extensive series of papers (see ud-Doula & Owocki, 2002; ud-Doula, 2003; Owocki & ud-Doula, 2004; ud-Doula et al., 2006, 2008, 2009, 2013), we have applied magnetohydrodynamical (MHD) simulations to understand the dynamics of magnetic wind channeling and the consequent hard X-ray emission. To disentangle competing processes, our philosophy thus far has been to focus on varying one parameter at a time. Thus, in our initial work (ud-Doula & Owocki, 2002), we demonstrated that the effect of the field on the wind depends largely on just a single *wind magnetic confinement parameter*, η_* which characterizes the competition between field and wind outflow energy density. In a following paper (ud-Doula et al., 2008) we extended this work by introducing rotation as a second parameter (as the ratio of equatorial velocity to orbital velocity, $W \equiv V_{\rm eq}/V_{\rm orb}$, where $V_{\rm orb} = \sqrt{GM/R_{\rm eq}}$) and showed how the magnetic channeling depends on these two parameters.

In practice, magnetic massive stars are often oblique rotators, which naturally leads – especially when rotation is rapid – to lateral structures that cannot be modeled by axisymmetric 2-D models. For field aligned or extremely slow rotators, statistical averages from 2D models can to a large extent mimic the behaviour in

3D (Sundqvist et al., 2012). But for rapid rotators with magnetic field tilted with respect to rotational axis, this is not option as axisymmetry is fully broken. As such, fully 3D MHD models of these massive stars become necessary.

However, such 3D models are not easy to compute due to a number of factors, including high computational costs and singularity along the polar axes that lead to unrealistically small timesteps. So, special care must be taken when performing such modelling

The main purpose of this study is to introduce one the first such fully 3D MHD models of obliquely rotating massive star wind models. We also introduce a correction to currently used reflective boundary condition that avoids many of the issues associated with singularity along polar axes in spherical geometry.

2 Numerical Methods

Most of our previous numerical models were performed using Zeus-3D or Zeus-MP codes, but here we use publicly available PLUTO code (version 4.2) (Mignone et al., 2007). It is a highly versatile modular code that includes a number of desirable features that is well suited for modern clusters.

Because the winds of massive stars are highly ionized and the competition between photoionization heating and radiative cooling keeps the wind close to the stellar effective temperature (Pauldrach, 1987; Drew, 1989), we can assume the wind is isothermal and model it with typical Magnetohydrodynamics (MHD) equations:

$$\frac{\partial \rho}{\partial t} + \boldsymbol{\nabla} \cdot (\rho \boldsymbol{v}) = 0, \tag{1}$$

$$\frac{\partial v}{\partial t} + (\boldsymbol{v} \cdot \nabla)\, \boldsymbol{v} + \frac{1}{4\pi\rho} \boldsymbol{B} \times (\nabla \times \boldsymbol{B}) + \frac{1}{\rho} \nabla p = \boldsymbol{g} + \boldsymbol{g}_{\rm lines} + \boldsymbol{F}_{\rm co}, \tag{2}$$

$$\frac{\partial \boldsymbol{B}}{\partial t} + \nabla \times (\boldsymbol{B} \times \boldsymbol{v}) = 0. \tag{3}$$

Where ρ, $\boldsymbol{v}$, $\boldsymbol{B}$, p, $\boldsymbol{g}$ and $\boldsymbol{F}_{\rm co}$ are, the density, velocity, magnetic field, pressure, acceleration due to gravity and acceleration due to the co-moving frame respectively. The additional acceleration term, $\boldsymbol{g}_{\rm lines}$, describes the acceleration due to line absorption (see next section). $\boldsymbol{F}_{\rm co}$ is the sum of both the centrifugal and Coriolis forces: $\boldsymbol{F}_{\rm co} = \boldsymbol{F}_{\rm centrifugal} + \boldsymbol{F}_{\rm coriolis}$ which are:

$$\boldsymbol{F}_{\rm centrifugal} = -\left[\boldsymbol{\Omega}_{\rm fr} \times (\boldsymbol{\Omega}_{\rm fr} \times \boldsymbol{R})\right], \tag{4}$$

and

$$\boldsymbol{F}_{\rm coriolis} = -2\left(\boldsymbol{\Omega}_{\rm fr} \times \boldsymbol{v}\right). \tag{5}$$

Here $\boldsymbol{\Omega}_{\rm fr}$ is the angular frequency of the rotating frame with $\boldsymbol{r}$ the radial distance vector.

As the wind is assumed to be isothermal, we close equations (1)–(3) using the relation:

$$p = \rho c_{\rm iso}^2, \tag{6}$$

in which $c_{\rm iso}$ is the isothermal sound speed, given by $c_{\rm iso}^2 = 2k_{\rm B}T/m_{\rm p}$, where $k_{\rm B}$ is the Boltzmann constant, $T_{\rm eff}$ the stellar surface effective temperature and $m_{\rm p}$ the proton mass.

2.1 Radial driving of wind outflow

This radial outflow arises from the strong radial driving of the line-force, $\mathbf{g}_{\rm lines}$. As in ud-Doula & Owocki (2002), we model this here in terms of the standard Castor, Abbott, & Klein (1975, hereafter CAK) formalism, corrected for the finite cone angle of the star, using a spherical expansion approximation for the local flow gradients (Pauldrach, Puls, Hummer, & Kudritzki, 1985; Friend & Abbott, 1986) and ignoring *non-radial* line-force components that can arise in a non-spherical outflow. Although such non-radial terms are typically only a few percent of the radial force, in non-magnetic models of rotating winds, they act without much competition in the lateral force balance, and so can have surprisingly strong effects on the wind channeling and rotation (Owocki, Cranmer, & Gayley, 1996; Gayley & Owocki, 2000). But in magnetic models with an already strong component of non-radial force, such terms are not very significant, and since their full inclusion substantially complicates both the numerical computation and the analysis of simulation results, we have elected to defer further consideration of such non-radial line-force terms to future studies.

By limiting our study to moderately fast rotation, half or less of the critical rate, we are also able to neglect the effects of stellar oblateness and gravity darkening.

2.2 Simulation

The chosen algorithm within PLUTO code was fully unsplit and 2nd order accurate in space and time, using linear reconstruction, Runge-Kutta time stepping and employed the HLL Riemann solver. The extended GLM divergence cleaning algorithm was used to ensure the $\nabla \cdot \boldsymbol{B} = 0$ condition.

2.3 Boundary conditions

Boundary conditions are difficult in MHD modelling and great care must be taken to avoid any unphysical outcomes. For most part, we closely followed boundary conditions outlined in ud-Doula & Owocki (2002) and Daley-Yates et al. (2019), with the latter describing the first obliquely rotating massive star winds, although their focus was radio emission from such objects.

In short, the outer radial boundary of the simulation is set to outflow. The inner radial boundary is set to 'inflow' such that the star is continually feeding material to the wind and therefore replenishing material in the simulation.

The velocity in the lower radial boundary is specified by linearly extrapolating back from the first 2 computational cells above the boundary, allowing the flow into the computational active zone to adjust to the conditions of the wind and permitting material to also re-enter the stellar surface as magnetically confined material follows field lines back to the stellar surface. We limit the maximum radial inflow/outflow speeds to the sound speed of the model. Specifying the boundary in this manner also allows the mass loading of the wind to self consistently adapt to the rotation of the star. Large rotational velocities can impact the mass-loss of a star. This is due to the effective gravity at the rotational equator being reduced relative to the poles, leading to material being lifted from the surface more easily.

The boundary of the lower and upper azimuthal direction is periodic. The upper and lower boundary of the polar direction was set to reflective so as not to act as

a sink for material. This final boundary condition is non-physical and a reflective polar boundary can lead to spurious heating or jets along the polar axis. There are several methods designed to overcome this numerical difficulty. One such method is known as π-boundary conditions in which the fluid quantities are translated π around the axis and vector values transformed such that material effectively passes over the pole. This method is implemented in the public codes Athena++ (White et al., 2016) and MPI-AMRVAC (Xia et al., 2018). PLUTO does not provide this functionality. But we avoid such issues by averaging fluid quantities over the poles and effectively smoothing over the anomalies.

In doing so, we first convert vectorial quantities to Cartesian, then average them over azimuth along polar axis. The final averaged quantity is then transformed back to spherical coordinates. For the case of velocity, we average over momentum and then modulate it with average density.

The isothermal assumption forces us to neglect behaviour due to both shock heating and radiative cooling. Both of which have been shown to play a role in the wind dynamics (ud-Doula et al., 2008, 2013). As such, this is a limitation of the present study and fully adiabatic simulations with cooling physics are the aim of future studies.

2.4 Numerical grid

For all our simulations we use spherical polar coordinate system. The numerical grid covered a physical extent of $r \in \{1, 15\}\, R_*$, $\theta \in \{0, \pi\}$ radians and $\phi \in \{0, 2\pi\}$ radians. For models with high magnetic field one has to ensure that the outer boundary is sufficiently far from the Alfvèn radius.

The simulations were performed using a stretched rectilinear spherical polar grid in which the physical volume was discretised with 200 cells in r, 150 cells in θ and 180 cells in ϕ. This leads to a cell size in the r direction which stretched from $\Delta r_1 \approx 0.0003\ R_*$ to $\Delta r_{200} \approx 0.511\ R_*$ with a constant stretching factor of 1.038. Both the θ and ϕ directions have uniform spacing. The stretching regime in the radial direction is required to resolve the sonic point of the wind, which is very close to the stellar surface. Typically, at least 5–10 grid points are required to resolve the sonic point to ensure correct amount of mass flow.

2.5 Stellar Parameters

We performed a number of simulations both in 3D and 2D to ensure the results are self-consistent. Here, we focus on only one 3D model with inclination angle between the magnetic field and rotation axes of 45°.

Following previous studies (ud-Doula & Owocki, 2002; ud-Doula et al., 2008), we use the stellar parameters of ζ Pup, a prototypical O-supergiant. In the absence of magnetic field, its mass loss was assumed to be about $3.0 \times 10^{-6} \mathrm{M}_\odot\,\mathrm{yr}^{-1}$. For our model here we assumed a dipolar magnetic field with polar strength of 1 kG corresponding to magnetic confinement of $\eta_* = 10$.

Assumed rotation is half the critical corresponding to about $250\,\mathrm{km\,s}^{-1}$ with axis aligned with z-axis. Magnetic field is inclined by 45° about y-axis and lies xz-plane.

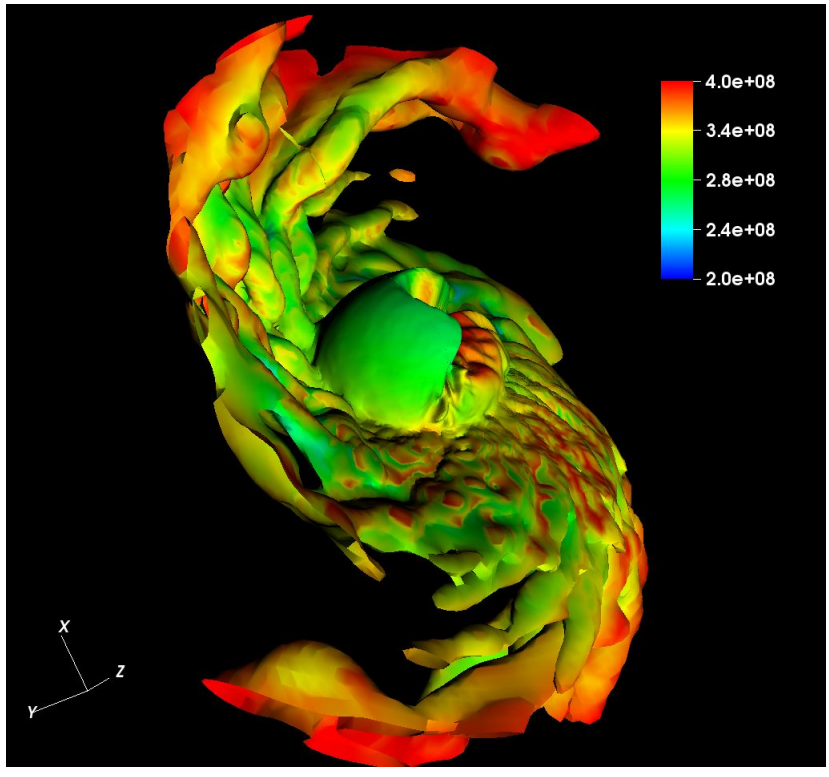

Fig. 1: Isodensity surface ($\log \rho = -15$) colored by wind speed in cgs units. This illustrates deformation fragmentation of the dense disk-like structure. The warped shape is due to combination of rotation and obliquity of the field.

2.6 Initial conditions

The initial conditions of the simulations were specified using the density and velocity profile equations assuming a spherically symmetric wind with CAK mass loss rate (Owocki & ud-Doula, 2004) and 'β'-law, i.e. $v(r) = v_\infty(1 - R_*/r)^\beta$ with $\beta = 0.8$ and $v_\infty \propto v_{\rm escape}$.

The magnetic field was initialised as a pure dipole, centred at the origin and rotated about the y-axis, in the xz-plane. We then evolve the model by letting the wind and magnetic field compete against each other. This configuration relaxes to quasi-steady state after only a few fluid crossing times.

3 3D MHD Simulation Results

Similar to our previous 2D MHD simulations, in the evolution immediately following the initial condition, the magnetic field channels wind material toward the tops of closed loops near the magnetic equator, where the collision with the opposite stream leads to a dense disk-like structure. But the strong magnetic field tends to torque the gas leading to co-rotation up to Alfvèn radius. Now, since the magnetic field axis is tilted with respect to the rotation axis, the dense structure quickly gets warped

especially far beyond Alfvèn radius as can be seen in Fig. 1.

Figure 1 shows isodensity surface at time 320 ks when the simulation already reached a quasi-steady state. The surface itself is colored with speed to capture overall dynamics of the wind. Despite being a still picture at a fixed time, it is clear that flow within is quite turbulent with high speed gas running into slow moving material.

Along the same vein, Fig. 2 shows magnetic field lines that were colored with speed with a background of density in logarithmic scale. As expected, material trapped inside magnetosphere is moving slowly, but flow along open field lines can reach substantial speeds. Note also how dense material breaks into smaller pieces far away from the stellar surface.

Figures 3 and 4 show a spherical slice at $r = 3R_*$ of speed and logarithm of density. Aim here is to illustrate topology of the wind with high density low speed magnetic equatorial region. Surprisingly, there is a rather low density high speed regions along polar axes. It is not clear why this is the case at this moment, and further analysis will be required to ensure it is not a numerical artifact. But in general magnetic polar flow is faster than magnetic equatorial flow, with finite rotational support at the base for this model, it might be easier for the gas to escape with higher speed and thus lower density.

Finally, Figs. 5 and 6 show slices along y-axis of speed and logarithm of density. Again, the region of high density with slow speed is clearly visible. But the dense structure fragments as it moves further away from the stellar surface due to combination of rotation and tilt of the magnetic field. A close inspection will also reveal that there are still some numerical artifacts along the axes. However, the issue is not severe enough to disrupt or influence the simulation significantly.

4 Conclusion and Future Works

Here we presented briefly one of the first 3D MHD simulations for an obliquely rotating massive star wind. We expect more models for specific targets in near future. One of the missing ingredients in this paper was the angular momentum loss. We expect to do a more in-depth and more systematic study to see how obliquity affects spindown time in magnetic massive stars.

Acknowledgements. A.uD. acknowledges support from NASA through Chandra Award number TM7-18001X issued by the Chandra X-ray Observatory Center, which is operated by the Smithsonian Astrophysical Observatory for and on behalf of NASA under contract NAS8-03060.

References

Babel, J., Montmerle, T., *ApJ* **485**, 29 (1997)

Castor, J. I., Abbott, D. C., Klein, R. I., *ApJ* **195**, 157 (1975)

Daley-Yates, S., Stevens, I. R., ud-Doula, A., *MNRAS* **489**, 3, 3251 (2019)

Drew, J. E., *ApJS* **71**, 267 (1989)

Feldmeier, A., Puls, J., Pauldrach, A. W. A., *A&A* **322**, 878 (1997)

Friend, D. B., Abbott, D. C., *ApJ* **311**, 701 (1986)

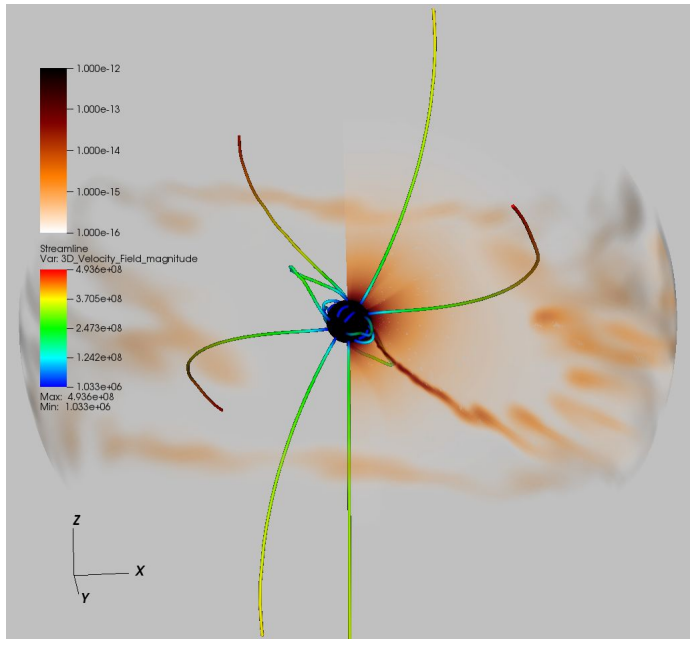

Fig. 2: Snapshot of magnetic field lines colored with wind speed in the background of logarithmic density at time 320 ks when the simulation reached a quasi-steady solution. Density structure within magnetosphere is similar to found in 2D models, but there are large scale breakouts, only small dense structures breaking through the field lines that eventually break into smaller pieces.

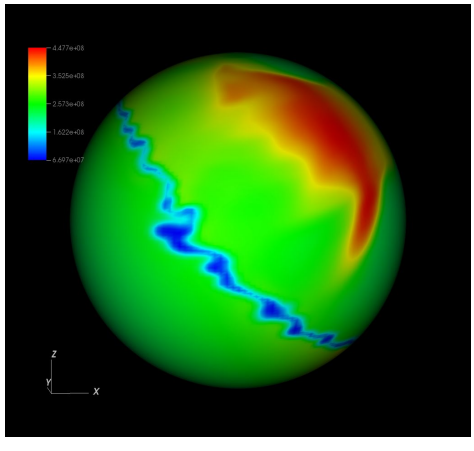

Fig. 3: Spherical slice at $r = 3R_*$. Color represents speed in cgs unit.

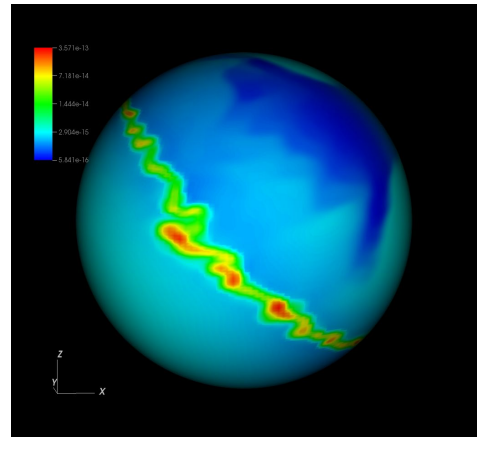

Fig. 4: Spherical slice at $r = 3R_*$. Color represents logarithm of density in cgs unit.

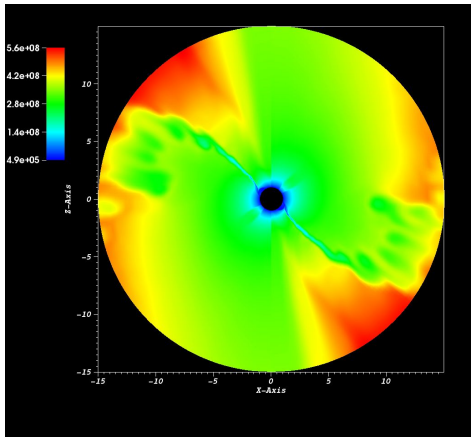

Fig. 5: Speed in xz-plane. Note slow moving dense material in magnetic equator.

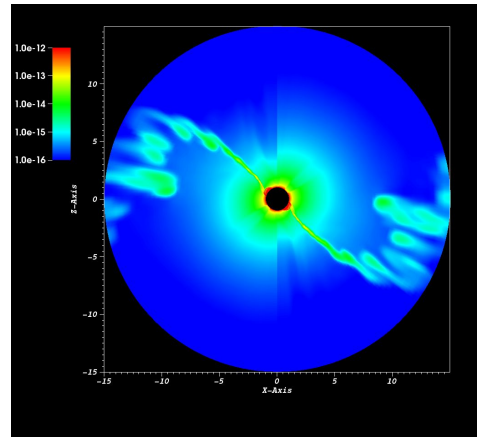

Fig. 6: Logarithm of density in xz-plane. Magnetic equator clearly visible.

Gayley, K. G., Owocki, S. P., *ApJ* **537**, 461 (2000)

Mignone, A., et al., *ApJS* **170**, 1, 228 (2007)

Nazé, Y., et al., *ApJS* **194**, 1, 7 (2011)

Owocki, S. P., Castor, J. I., Rybicki, G. B., *ApJ* **335**, 914 (1988)

Owocki, S. P., Cranmer, S. R., Gayley, K. G., *ApJ* **472**, L115+ (1996)

Owocki, S. P., ud-Doula, A., *ApJ* **600**, 1004 (2004)

Pauldrach, A., *A&A* **183**, 295 (1987)

Pauldrach, A., Puls, J., Hummer, D. G., Kudritzki, R. P., *A&A* **148**, L1 (1985)

Sundqvist, J. O., et al., *MNRAS* **423**, L21 (2012)

Townsley, L. K., et al., *ApJS* **194**, 1, 1 (2011)

ud-Doula, A., The effects of magnetic fields and field-aligned rotation on line-driven hot-star winds, Ph.D. thesis, University of Delaware (2003)

ud-Doula, A., Owocki, S. P., *ApJ* **576**, 413 (2002)

ud-Doula, A., Owocki, S. P., Townsend, R. H. D., *MNRAS* **385**, 97 (2008)

ud-Doula, A., Owocki, S. P., Townsend, R. H. D., *MNRAS* **392**, 1022 (2009)

ud-Doula, A., Townsend, R. H. D., Owocki, S. P., *ApJ* **640**, L191 (2006)

ud-Doula, A., et al., *MNRAS* **428**, 3, 2723 (2013)

Wade, G. A., et al., *MNRAS* **456**, 1, 2 (2016)

White, C. J., Stone, J. M., Gammie, C. F., *ApJS* **225**, 2, 22 (2016)

Xia, C., et al., *ApJS* **234**, 2, 30 (2018)